

ORIGINAL ARTICLE

Open Access



Bending responses of self-shaping wood bilayers: comparison between adsorption and desorption processes

Hui Peng¹, Zhiting Liu¹, Jianyi Zhu¹, Jiali Jiang², Jianxiong Lyu^{1,2} and Tianyi Zhan^{1*}

Abstract

Inspired by biological materials, the self-shaping wood composites induced by relative humidity (RH) have been investigated over the last decade. In this study, a wood bilayer was fabricated by assembling two layers with perpendicular fiber orientation in a series of thickness ratios and initial moisture contents (iMC). The self-shaping response of the wood bilayer was explored as a function of its configuration, and the discrepancies between moisture adsorption and desorption processes were clarified. Higher iMC limited the evolution of curvature. During both the adsorption and desorption processes, a reversed bending response was observed, and there was a hysteretic bending behavior between them. Repeatable bending was achieved during the cyclic ad/desorption process, and a larger hysteresis loop was observed at a lower thickness ratio. Finite-element analysis showed that the maximum stress occurred at the interface between the active and passive layers, and larger thickness ratios had lower maximum stress. In addition, the bilayer composed of a 200 μm passive layer and a 400 μm active layer with 0.6% iMC was found to be the most sensitive to RH change. The results of this study elucidate the moisture-dependent bending response of wood bilayers and provide the possibility of precisely controlling the curvature of self-shaping wood composites in industrial applications.

Keywords Self-shaping, Wood bilayer, Adsorption/desorption, Hysteresis

Introduction

The dimensional instability of wood with moisture changes is considered to be a drawback and limitation for its application in civil engineering [1]. Various approaches have been developed to reduce the dimensional instability, such as using expensive equipment for structural adaptation or chemical agents for modification. However, the hygroexpansion of wood has recently been turned into an advantage in the field of self-shaping

actuators [2–4]. The self-shaping mechanism is inspired by natural plant actuators with a bilayer structure such as pine cones who open during a decrease in relative humidity (RH) and close during an increase in RH [5–7]. This shape change is originally from the stress gradient due to the bilayer structure, which is composed of two layers (active and passive layers) exhibiting differential dimensional changes in response to moisture, i.e., anisotropic hygroexpansion within the bilayer structure [8–10]. The active layer with a higher hygroexpansion coefficient strongly reacts to moisture changes, whereas the passive layer is less sensitive to moisture due to the lower coefficient [11]. When moisture uptake or loss, the stress gradient involved in the bilayer structure would turn differential hygroexpansion strain into a passive bend [12, 13].

*Correspondence:

Tianyi Zhan
tyzhan@njfu.edu.cn

¹ Co-Innovation Center of Efficient Processing and Utilization of Forest Resources, Nanjing Forestry University, 210037 Nanjing, People's Republic of China

² Research Institute of Wood Industry of Chinese Academy of Forestry, 100091 Beijing, People's Republic of China



© The Author(s) 2023. **Open Access** This article is licensed under a Creative Commons Attribution 4.0 International License, which permits use, sharing, adaptation, distribution and reproduction in any medium or format, as long as you give appropriate credit to the original author(s) and the source, provide a link to the Creative Commons licence, and indicate if changes were made. The images or other third party material in this article are included in the article's Creative Commons licence, unless indicated otherwise in a credit line to the material. If material is not included in the article's Creative Commons licence and your intended use is not permitted by statutory regulation or exceeds the permitted use, you will need to obtain permission directly from the copyright holder. To view a copy of this licence, visit <http://creativecommons.org/licenses/by/4.0/>.

Wood, as an anisotropic natural material, consists of highly crystalline cellulose microfibrils and amorphous lignin–hemicellulose matrix [14, 15]. Since cellulose microfibrils almost aligned along longitudinal direction are responsible for the mechanical support in wood and hardly swelling or shrinkage, the hygroexpansion exhibits pronounced difference in longitudinal, radial and tangential directions [16–18]. Maximum hygroexpansion could be found in tangential direction followed by radial direction, while the hygroexpansion in the longitudinal direction is at least an order of magnitude smaller than that in the transverse direction [1]. This orthotropic hygroexpansion property enables wood to be used as a material for fabricating RH-driven self-shaping bilayers that consist of two wood monolayers with different grain orientation and can bend reversibly upon RH changes [19–21].

The self-shaping wood bilayers in response to changes in RH have been explored and fabricated into a series of products, such as the “Urbach tower” [22, 23], smart building ventilations—hygroscope or hygroskin [24–26], and self-propelling robot [27, 28]. During the manufacturing of wood bilayers from the monolayer with initial moisture content (iMC) by means of hot-pressing, thermoplastic deformation occurred in the wood bilayers, which then affected the bending response of the bilayers. More importantly, the bending response of the bilayers is mainly driven by RH changes. When wood bilayers are used as hygrometers in the form of sensors or actuators, it is important to precisely describe the bending curvature of bilayers at any RH condition. Due to the distinct moisture sorption kinetics behavior of wood between the adsorption and desorption isotherms [29, 30], the bending response of wood bilayers would be of interest during the adsorption and desorption processes despite the same RH. Moreover, the effect of cyclic RH conditions on the bending behavior of wood bilayers is also important for wood bilayer applications. To explore the bending behavior, the bilayer motion response to fluctuations in RH can be tracked by a camera, and image analysis software has been verified as an effective test method to perform the image treatment and bending curvature measurement [31–33]. The stress gradient within bilayers, responsible for the bending response to RH change, is hard to detect due to the limited technology. Finite-element analysis (FEA) is a widely used numerical method for analyzing stress distribution in structures, including wooden materials. Sophisticated constitutive models have been developed to capture the nonlinear, anisotropic, and time-dependent behavior of wood [34, 35]. Obtaining material properties through experimental testing and integrating them into FEA simulations has been a key focus for researchers. In the case of wooden bilayers, the material can be divided into small elements with

varying properties. This approach allows for simulating the stress gradient within the bilayer structure based on the physical or mechanical properties of both the active and passive layers [22].

Thus, this paper was aimed at comparing the bending response of wood bilayers between adsorption and desorption processes. The bending curvature of the wood bilayers fabricated was measured by ImageJ software [36] during adsorption, desorption, and cyclic adsorption–desorption processes. We designed wood bilayers with several variables, including the thickness of each layer, i.e., the passive to active layer thickness ratio (m , T_p/T_a), and iMC of each layer prior to assembling. The bending ability of the manufactured bilayers was checked first, and then the critical RH region to reverse bend was marked as well. Furthermore, the stress gradient of the self-shaping wood bilayers in response to RH change was modeled using the FEA.

Materials and methods

Wood bilayers manufacturing and conditioning

Scots pine (*Pinus sylvestris* var. *mongolica* Litv) was selected to fabricate the bilayers. The clear rods from sapwood were prepared with the dimensions of 20 mm (longitudinal, L) × 5 mm (radial, R) × 20 mm (tangential, T), without any visual defects and knots. The average density and moisture content under air-dried condition were 0.47 g/cm³ and 11%, respectively.

The different orientations of the grain in the passive and active layers are mainly responsible for the deformation of the bilayer. The passive and active layers were cut using diamond wire saw (DWS100, Diamond WireTec, Germany) in the LR plane (L-direction along the x-axis of the bilayer) and the cross-plane (T-direction along the x-axis of the bilayer), respectively, with a length of 20 mm and a width of 5 mm (Fig. 1). 200 μm and 400 μm-thick passive layers and 200 μm, 400 μm, and 800 μm-thick active layers were prepared (Table 1). The active or passive layers were divided into three groups for adjusting iMC. The three groups were conditioned at a constant humidity of 0%, 75%, and 100% RH by storing in sealed containers over anhydrous phosphorus pentoxide (P₂O₅), saturated sodium chloride (NaCl) solution, and deionized water. After 9 weeks, the steady mass of the layers was obtained, and the corresponding iMC was about 0.6, 12, and 22% for 0%, 75% and 100% RH, respectively.

After adjusting iMC, the active and passive layers with the same iMC value were bonded with phenolic resin (Dynea Guangdong Co. Ltd., China) by hot-pressing. The spreading amount of the resin was 100 g/m², and the water content of the phenolic resin was 50%. Figure 1 shows the hot-pressing process. To minimize the effect of hot-pressing on the thickness, the active layer and passive

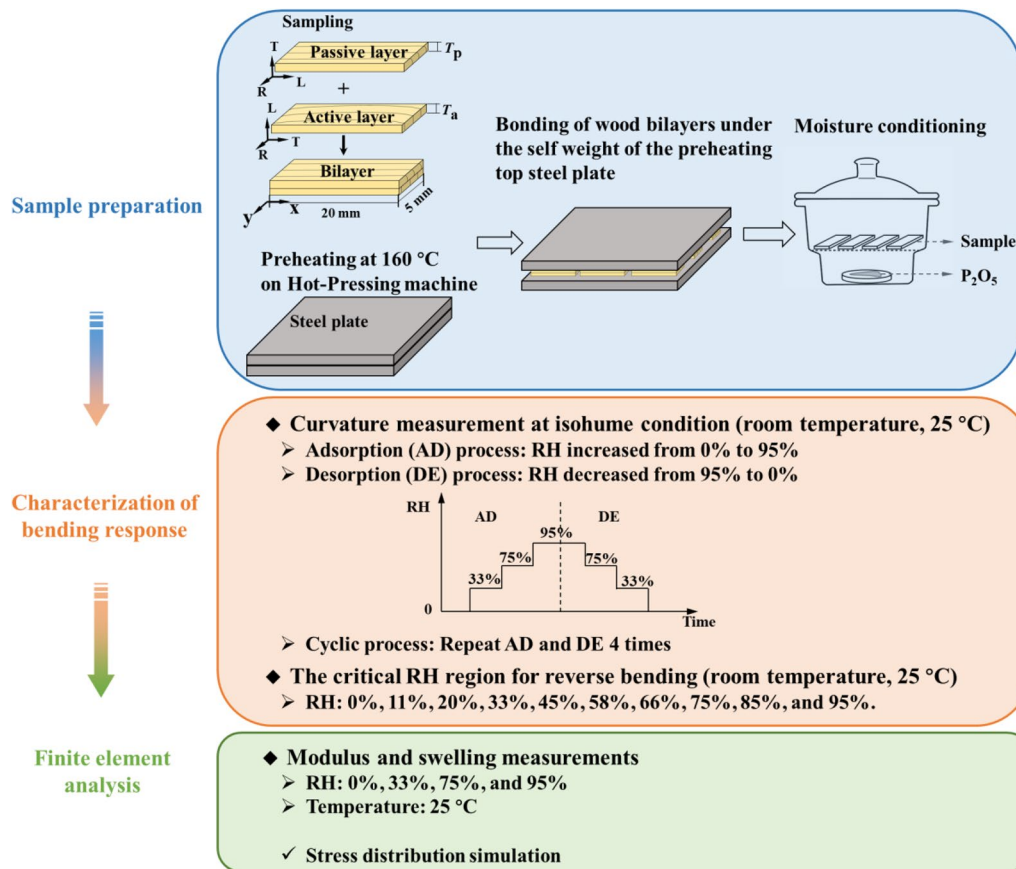


Fig. 1 Schematic illustration of the sample preparation and characterization

Table 1 Thickness ratios for the different combinations of thickness

Thickness of passive layer, T_p	Thickness ratio $m (T_p/T_a)$	
200 μm	0.5 (200/400)	1 (200/200)
400 μm	0.5 (400/800)	1 (400/400)

T_a , thickness of active layer

layer were bounded under the self-weight of preheating top steel plate (2 kg) at 160 °C for 1 min (Fig. 1). Moreover, the actual thickness was influenced by RH fluctuations in the process of bilayers bending measurements due to hygroexpansion. Thereafter, the thicknesses of active or passive layers after hot-pressing can be considered as nominal thickness. The passive to active layer thickness ratio $m (T_p/T_a)$ was selected as 0.5 and 1 (Table 1). Thus, the bilayers with a length of 20 mm along the x-axis and a width (y-dimension) of 5 mm were obtained at the thickness ratios of 0.5 and 1. Prior to tests, all bilayers were dried in sealed containers over P_2O_5 (Fig. 1).

Characterization of bending response

Curvature measurement during ad/desorption processes

The wood bilayers were fixed with a clamp in a home-made climate chamber at the room temperature of 25 °C (Fig. 2a). The fixation by the clamp had no negative influence for the bending along the lengthwise direction of the bilayer [32]. The profile of the bilayer was captured by a digital camera (Fig. 2c) to track changes in bending. The image was then analyzed using the ImageJ software (National Institute of Health, USA) to calculate bending curvature [36]. The curvature measurement scheme in Fig. 2b illustrated that the evolution of the bilayer was fitted to a “circle” function, and the curvature (K) could be calculated using the radius (R) of the fitted circle. In each bilayer, the active layer faced the left side, and negative curvature was defined when the bilayer was in a left-bending position (i.e., bending with the active layer inwards) (Fig. 2c). Positive curvature was noted when the bilayer was bent with the passive layer inwards.

The bending ability of bilayers was evaluated by curvature changes during adsorption, desorption and cyclic

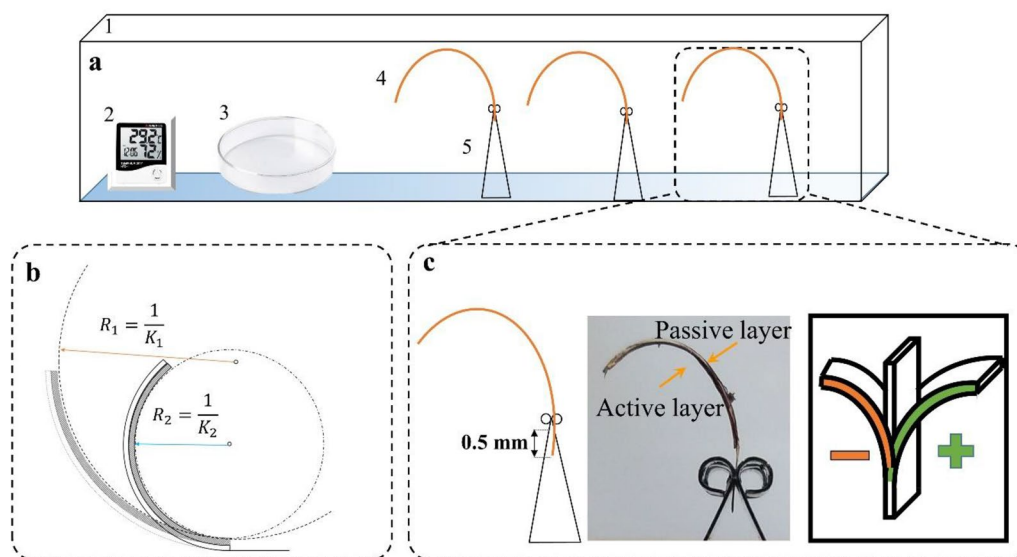


Fig. 2 a Schematic diagram of the experimental device (1. Climate chamber, 2. Digital temperature and humidity sensor, 3. Desiccator containing P₂O₅ or saturated solution, 4. Bilayer sample, 5. Vertical clamp); b Calculation of curvature K₁ or K₂ of bilayer before and after deformation based on the radius R₁ or R₂ of the fitted circle; c sample clamping schematic diagram with negative curvature value (the bilayer in a left-bending position, i.e., bending with the active layer inwards)

processes by controlling RH in the climate chamber. The curvature hysteresis defined as the curvature difference at desorption process and adsorption process ($|K_{de} - K_{ad}|$) for a given RH was evaluated as well. Isohume conditions were adjusted using P₂O₅ (for 0% RH) or a series of saturated salt solutions (for moist conditions). Figure 1 presents the test scheme for curvature measurement. All tests were conducted at room temperature (25 °C). For the adsorption or desorption process, the RH was adjusted to 0%, 33%, 75% and 95%, progressively. In the case of the cyclic process, RH was run started at 0% RH and increased stepwise to 33%, 75%, and 95%, and then decreased stepwise to 75%, 33%, and 0% followed by a period of 3 cyclic changes. The samples were maintained at each humidity condition until the curvature change reached 0.001 μm⁻¹ per 24 h. The average curvature was averaged from 5 replicates.

Determination of critical RH region for reverse bending

The reverse bending phenomenon can be observed for the bilayers during both the adsorption and desorption processes. The RH region when reverse bending occurs was defined as critical RH (RH₀) region. The RH₀ region was obtained by observing the bending direction of bilayers at a series of RH. The RH isohume conditions were set at 11%, 20%, 33%, 45%, 58%, 66%, 75%, 85%, and 95% RH, controlling by saturated solutions of lithium chloride (LiCl), potassium acetate (KC₂H₃O₂), magnesium

chloride (MgCl₂), potassium nitrite (KNO₂), sodium bromide (NaBr), sodium nitrite (NaNO₂), sodium chloride (NaCl), potassium chloride (KCl), and sodium carbonate (Na₂CO₃).

Finite-element analysis (FEA)

The stress distribution was modeled using FEA software (student version, <https://www.ansys.com/academic/students>). The dimensions of the model were consistent with the actual size. The modulus and swelling of the dried active and passive layers (0.6% MC) at 0%, 33%, 75% and 95% RH were measured in tensile mode by micro-mechanical analyzer (HCS350G-TNS, Instec, USA) and given in Table 2. Strain simulation was applied using the differential swelling between the active and passive layers at RH = 33%, 75%, or 95%. The stress distribution was then obtained, especially within

Table 2 Modulus and swelling for active and passive layers under different RH conditions

RH/%	MC/%	Modulus/MPa		Swelling/%	
		Passive layer	Active layer	Passive layer	Active layer
0	0.6	4602	128	0	0
33	7.7	4322	86	0.15	5.04
75	12.5	4150	80	0.20	6.81
95	20.3	3860	75	0.24	8.12

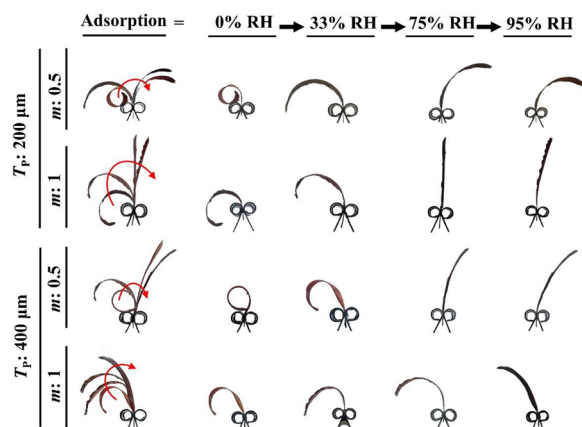


Fig. 3 The bending evolution of bilayers manufactured from the monolayers with 12% iMC when the relative humidity increased from dry (0% RH) to a wet environment (95% RH) at 25 °C. T_p , the thickness of passive layer; m , passive to active layer thickness ratio

or along the interface between the active and passive layers.

Results and discussion

Bending response during adsorption process

Curvature changes

The differential swelling behavior between active and passive layers allows for asymmetric deformation along the lengthwise direction of the bilayer, resulting in bending. The typical bending evolution of the bilayer with 12% iMC is shown in Fig. 3. During the adsorption process, bilayers displayed a pronounced actuation authority regardless of the bilayer thickness. The bilayers reached their maximum left-bending position (i.e., negative curvature in Fig. 2c) at the beginning of the adsorption (RH=0%) and then gradually bent rightward with increasing RH. Except for the bilayer with a thickness ratio of 1 (both the passive and active layers were 400 μm-thick), the others had the maximum right-bending position (positive curvature) at the highest RH. In other words, these bilayers bent from the active layer inwards to the passive layer inwards during the adsorption process. The bending response is related to the differential swelling of the active and passive layers upon water uptake. The left-bending position of bilayers at low RH level indicated that the swelling of the active layer could not catch up with the length of the passive layer, and the passive layer is longitudinally loaded in tension. The right-bending position of bilayers at high RH level indicated that the active layer is excessively swelled compared to the passive layer, and the passive layer is longitudinally loaded in compressive mode.

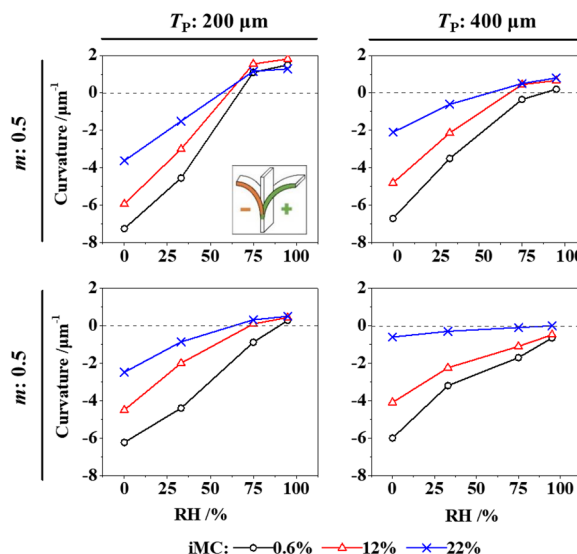


Fig. 4 The curvature evolution for four investigated bilayer configurations manufactured from the monolayers with 0.6%, 12% and 22% iMC during adsorption. T_p , the thickness of passive layer; m , passive to active layer thickness ratio

The curvature evolution as a function of RH is presented in Fig. 4. The negative curvature value indicated the left-bending position in Figs. 2c and 3, i.e., bending with the active layer inwards. During the adsorption process, the curvature of the bilayers evolved nonlinearly with the increasing RH, regardless of the bilayers' configuration. The higher the RH levels, the less pronounced the bending of the bilayers was, due to the influence of swelling stress on water uptake [32, 37].

The iMC and thickness effects

The bilayers with lower iMC had a greater curvature (Fig. 4). To elucidate the influence of iMC on the bending response, the relative curvature (ΔK) was calculated by the curvature difference at 95% and 0% RH ($\Delta K = |K_{95\%} - K_{0\%}|$). Table 3 shows that ΔK increased as the iMC decreased. During the manufacturing process of bilayers by hot-pressing, thermoplastic strain occurred due to the plasticization effect of moisture, which led to an unrecoverable strain and internal stress. Therefore, the humidity-induced bending curvature was lower at high iMC.

Higher values of ΔK were achieved when m was 0.5 (Table 3), irrespective of iMC. This result was consistent with previous studies on other bi-layered composites [12, 38] based on Timoshenko's model [8]. As stated by Holstov [24], curvature of bilayer depends on the thickness ratio m , the passive to active layer stiffness ratio, and the total thickness of the bilayer. At a given m value, a slightly higher ΔK was found in the sample with a 200 μm-thick

Table 3 The relative curvature ΔK for four investigated bilayer configurations manufactured from the monolayers with 0.6%, 12% and 22% iMC

iMC	Adsorption				Desorption			
	0.5, 200/400	1, 200/200	0.5, 400/800	1, 400/400	0.5, 200/400	1, 200/200	0.5, 400/800	1, 400/400
0.6%	8.74 (0.19)	6.51 (0.14)	6.90 (0.15)	5.34 (0.14)	6.62 (0.17)	5.28 (0.12)	5.33 (0.14)	4.12 (0.10)
12%	7.74 (0.15)	4.93 (0.11)	5.46 (0.13)	3.61 (0.07)	5.47 (0.15)	4.30 (0.10)	4.66 (0.11)	3.31 (0.10)
22%	4.91 (0.1)	2.99 (0.08)	2.90 (0.05)	0.60 (0.03)	3.51 (0.09)	2.18 (0.06)	2.30 (0.04)	0.29 (0.02)

$\Delta K = |K_{95\%} - K_{0\%}|$, standard error in parentheses

passive layer compared to that with a 400 μm -thick passive layer, regardless of iMC, explained from the viewpoint of the size effect. On the one hand, a positive relationship of stiffness to sample thickness over the 70–1000 μm range has been reported for wood cut along the grain [39, 40], while the stiffness of wood cut across the grain has rarely related to thickness. For the bilayer composed of a passive layer along grain direction and an active layer across grain (Fig. 1), thick passive layer with large stiffness would cause the bilayer to consume more energy to resist the stiffness of passive layer, and then the bending capacity of bilayer is weakened, i.e., low ΔK value for the bilayer with 400 μm -thick passive layer. On the other hand, the total thickness of the bilayer has a negative effect on the curvature, which may be due to the gravity hindering the bending change of bilayer [24]. As a consequence, low ΔK value was observed for the thick bilayers at a given m value.

The reversed bending phenomenon was observed for all cases except the case with $m = 1$ ($T_p/T_a = 400/400$) in Fig. 3, meaning that there was a specific time when the curvature was about 0 in a certain RH region. Higher RH_0 regions were found at lower iMCs for all configurations (Fig. 5). The bilayers with an m value of 0.5 displayed lower RH_0 regions, regardless of the thickness of the passive layer. In addition, the lowest RH_0 region was found in the bilayer consisting of a 200 μm -thick passive layer and a 400 μm -thick active layer ($m = 0.5$) compared to other bilayer configurations (Fig. 5). Based on the ΔK value and RH_0 region analysis, the results suggested that the bilayer with a configuration of a 200 μm -thick passive layer and a 400 μm -thick active layer with 0.6% iMC was sensitive to RH change during adsorption.

Bending response during desorption
Curvature changes

Similar to the adsorption process, bilayers exhibited bending evolution during the desorption process (Fig. 6).

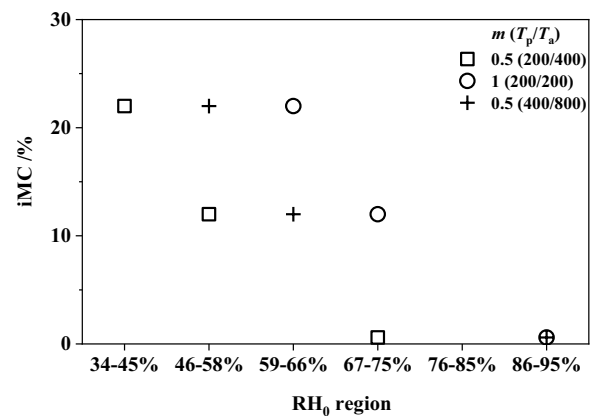


Fig. 5 The critical RH (RH_0) region during adsorption for bilayers with different passive to active layer thickness ratio ($m, T_p/T_a$) at 0.6%, 12% and 22% iMC

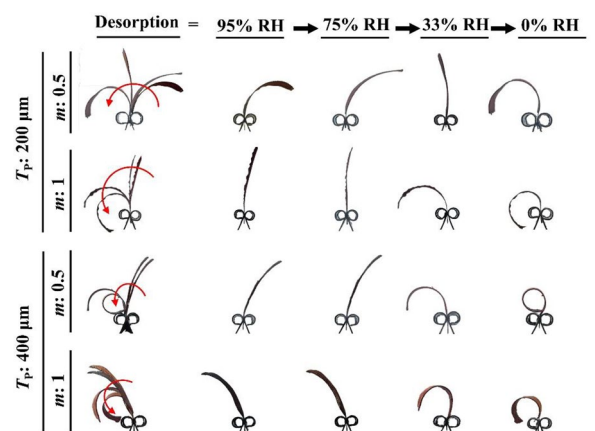


Fig. 6 The bending evolution of bilayers manufactured from the monolayers with 12% iMC when the relative humidity is decreased from wet environment (95% RH) to dry (0% RH) at 25 °C. T_p , the thickness of passive layer; m , passive to active layer thickness ratio

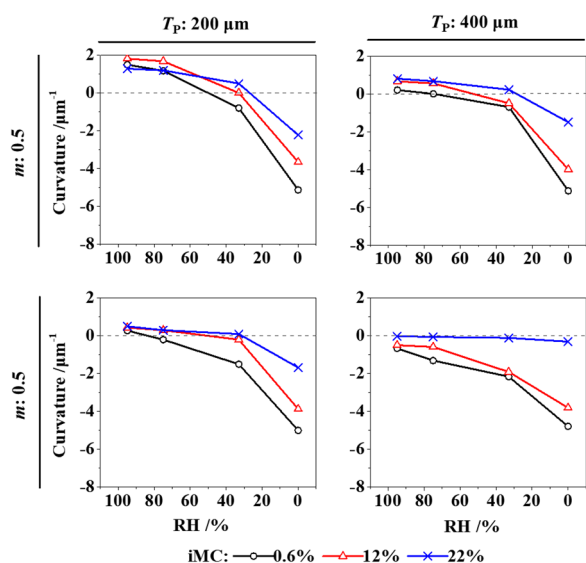


Fig. 7 The curvature evolution for four investigated bilayer configurations manufactured from the monolayers with 0.6%, 12% and 22% iMC during desorption. T_p , the thickness of passive layer; m , passive to active layer thickness ratio

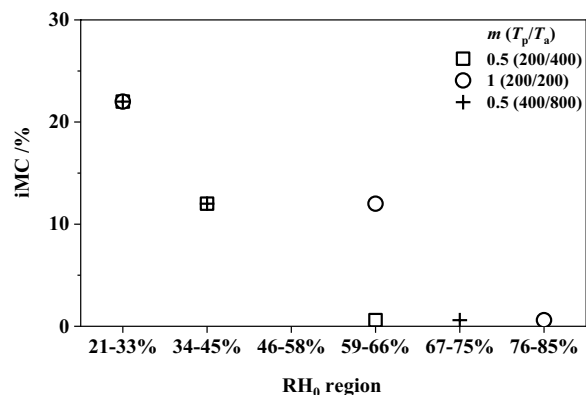


Fig. 8 The critical RH (RH_0) region during desorption for bilayers with different passive to active layer thickness ratio ($m, T_p/T_a$) at 0.6%, 12% and 22% iMC

The bilayers gradually bent rightward during adsorption (Fig. 4) and leftward while desorption (Fig. 6), demonstrating the ability of the prepared bilayers to undergo reversible bending actuation. When humid environments changed from wet to dry, the curvature evolution for all configurations is presented in Fig. 7. A nonlinear relationship between RH and curvature was found for all bilayer configurations, exhibiting slow reactivity of bilayers at high RH regions.

The iMC and thickness effects

The bilayers with an m value of 0.5 exhibited high curvature, regardless of the thickness and iMC of the passive layer. With an increase in iMC, the relative curvature ΔK decreased (Table 3). At a given iMC, greater ΔK was observed using an m value of 0.5 instead of 1. The distinct curvature between the samples with 200 μm and 400 μm -thick passive layers was attributed to thickness-dependent stiffness. These findings were similar to the results during adsorption. Thus, bilayers composed of 200 μm -thick passive layers at an m value of 0.5 were more sensitive to RH changes during both sorption processes.

Figure 8 shows the RH_0 region for reversed bending during the desorption process. The bilayers composed of 400 μm -thick passive layer had RH_0 region only when m value was 0.5 in this study. The higher the iMCs, the lower the RH_0 regions were found (Fig. 8). In addition, low iMC can promote the scatter of the RH_0 region with different values of m . Comparing with the adsorption process (Fig. 5), a low RH_0 region was found in the desorption process (Fig. 8), indicating discrepancies in the bending response between the adsorption and desorption processes.

To understand the humidity-induced bending behavior, all the curvature data during the adsorption and desorption processes were included in Fig. 9. The bending deformation (not only the curvature but also the ΔK) during adsorption was significantly greater than during desorption. The bending complexity generally arises from the inhomogeneous distribution of stress along the bilayer or across its thickness due to the differential expansion between L and T directions [9]. The hysteresis was probably due to the different stress gradient within the bilayers between the adsorption and desorption processes [32, 36]. The hysteresis was more pronounced at a low iMC for all four configurations.

Bending response during cyclic process

The curvature measurement during cyclic adsorption–desorption process was conducted to clarify the effectiveness of the bilayers actuators. Figure 10 displays the reversibility of the bending during 4 cyclic processes. Neither cracking in the wood layers nor delamination at the interface of bonding area was observed during the cyclic process, indicating no visual impact occurred for the bilayers manufactured. The first adsorption–desorption cycle might wear in the asymmetric self-shaping system and leave the dried bilayer in an unrecovered curvature, i.e., the initial curvature during adsorption could not be achieved. Subsequent cycles led to approximately repeatable and reproducible bending behavior. A greater

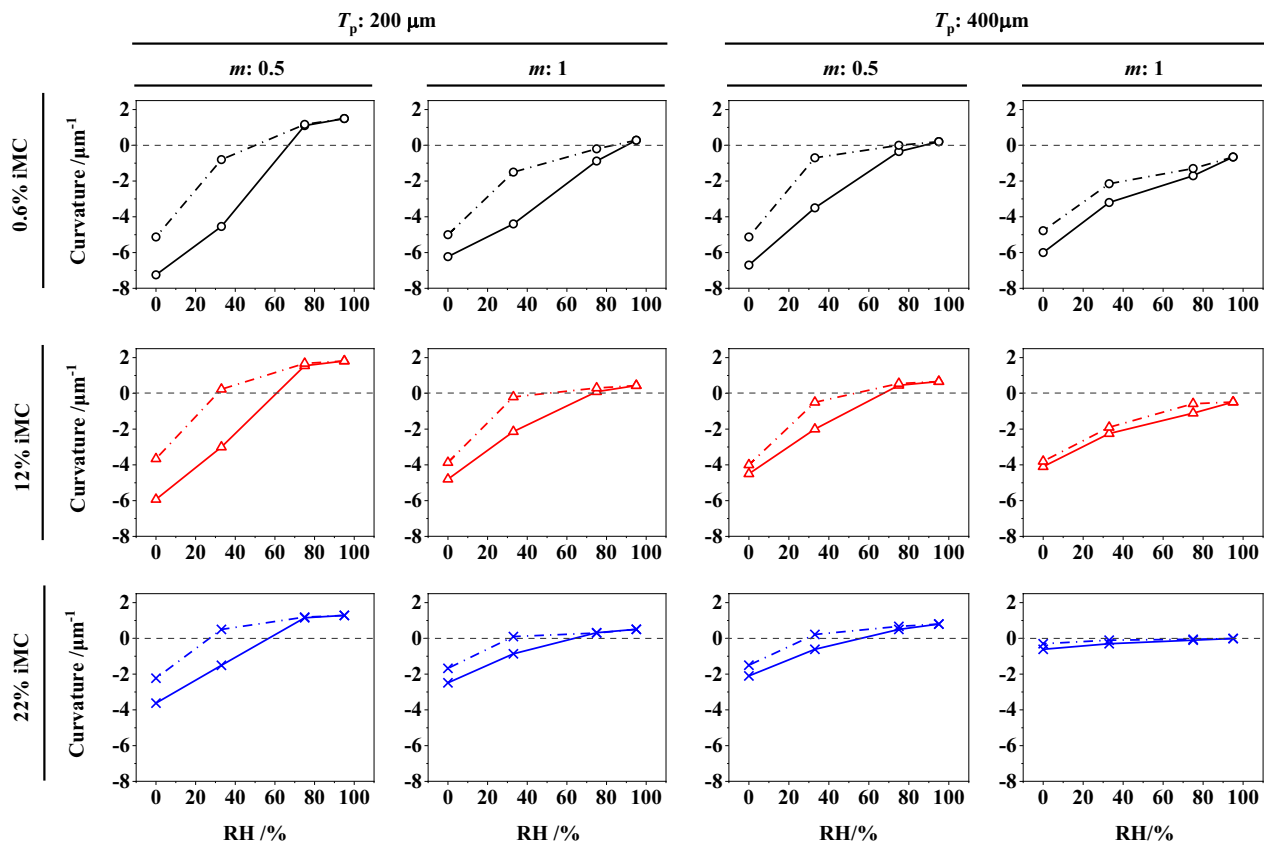


Fig. 9 The curvature evolution for four investigated bilayer configurations manufactured from the monolayers with 0.6%, 12% and 22% iMC during adsorption (solid line) and desorption process (dotted line). T_p , the thickness of passive layer; m , passive to active layer thickness ratio

bending amplitude (the ΔK at fourth cycle process) was observed for the bilayers with 200 μm -thick passive layer at an m value of 0.5 compared to the other three configurations. However, the curvature amplitude was found to be higher for the bilayers with the thinner passive layer at a given m value, attributed to the aforementioned size effect on stiffness and stress relaxation.

For a given passive layer thickness, larger hysteresis loops were found at a lower m value, i.e., with a thick active layer (Fig. 10). This result was similar to the studies on sorption hysteresis [41], suggesting that matrix relaxation was responsible for hysteresis behavior. The matrix relaxation during desorption is kinetically hindered and cannot go back to the state it was in adsorption, because adsorption process led to inelastic expansion [42]. The richer the matrix, the more pronounced the hysteresis behavior [41]. Furthermore, matrix plays a decisive role in the swelling/shrinkage along the T-direction (i.e., active layer) [43]. Thus, it seems like the thicker the active layer is, the larger the hysteresis loops.

FEA results

The stress nephograms simulated by FEA demonstrated a distinct stress distribution along the thickness direction (Fig. 11). Compared with the passive layer, less stress was found for the active layer. The interface between the active and the passive layer (interface A–P) had the highest stress concentration, as shown in Fig. 11. During adsorption, maximum tensile stresses (RH=33%) of around 24 MPa for $m=1$ (Fig. 11a) and 20 MPa for $m=0.5$ (Fig. 11b) were found at the interface.

The bilayer model was an optimized structure that allowed for large unconstrained deformations and prevented delamination even with large variations in wood MC [22]. The active layer shrank and swelled with the changes of RH, driving the passive layer to deform. Therefore, a stress gradient was generated, and a neutral layer appeared along the central part of the passive layer. Regardless of the m value, the interface stress decreased initially and then increased with increasing RH, which was in accordance with the change in curvature. For a given passive layer thickness, the thicker the active layer (i.e., lower m value), the greater the interface stress can be found.

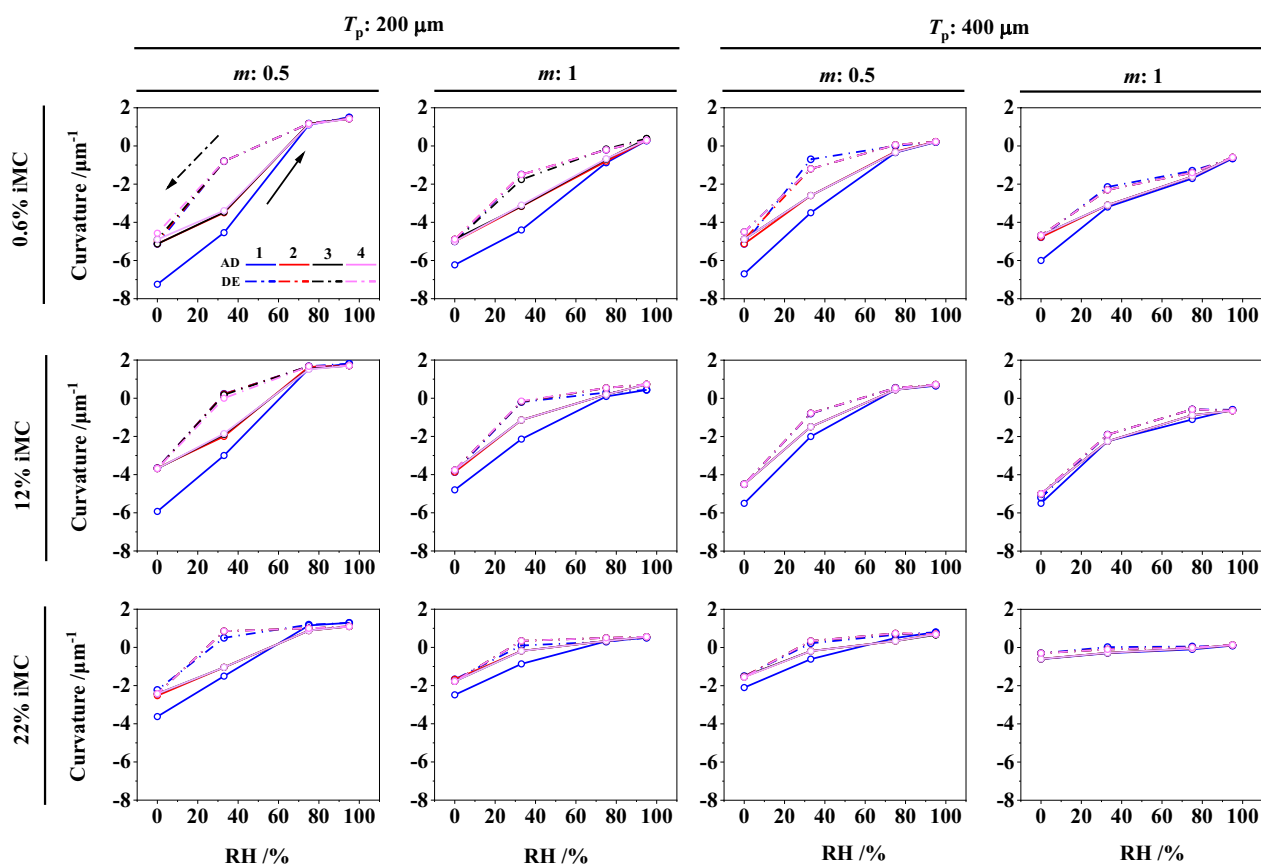


Fig. 10 The curvature evolution for four investigated bilayer configurations manufactured from the monolayers with 0.6%, 12% and 22% iMC during cyclic process. T_p , the thickness of passive layer; m , passive to active layer thickness ratio

Conclusion

The natural anisotropy of wood and its sensitive to moisture was utilized to manufacture self-shaping bilayer induced by the changes of ambient humidity. Wooden bilayers were made from two layers with perpendicular fiber orientation, i.e., an active layer along T-direction and a passive layer along L-direction. The bending motion of the bilayers during RH change was attributed to the differential lengthwise expansion between the active and passive layers. The differential curvature evolution of the wood bilayers was observed during adsorption, desorption, and cyclic processes.

During the adsorption and desorption processes, a nonlinear relationship between RH and curvature was found irrespective of the bilayer configurations, exhibiting slow reactivity of bilayers at high RH regions. The high values of iMC limited the curvature evolution due to the thermoplastic effect induced by hot-pressing. The bending direction reversed during RH changes for all bilayers except the configuration with 400 μm-thick

passive layer and 400 μm-thick active layer. The lower the iMC, the higher the critical RH region related to reversed bending. However, the critical RH region during adsorption was higher than that during desorption due to hysteresis behavior. During the cyclic process, the bending deformation during desorption was unable to fully relax to the state it stayed in the adsorption. A larger hysteresis loop was found at a lower thickness ratio for a given passive layer thickness. FEA results showed that the maximum stress occurred at the interface between the active and passive layer. A sensitive humidity-induced bilayer was obtained at the optimal configuration of a 200 μm passive layer and a 400 μm active layer with 0.6% iMC. The results of this study showed that self-shaping wood bilayers have the ability to bend automatically in specific environments without energy input and external force. The knowledge of the different self-shaping responses between adsorption and desorption allows for the potential application to precisely design and control the curvature in humidity-induced self-shaping wood bilayers. For example, the design of handicrafts with specific curvature: adjust the humidity to control the curvature, or

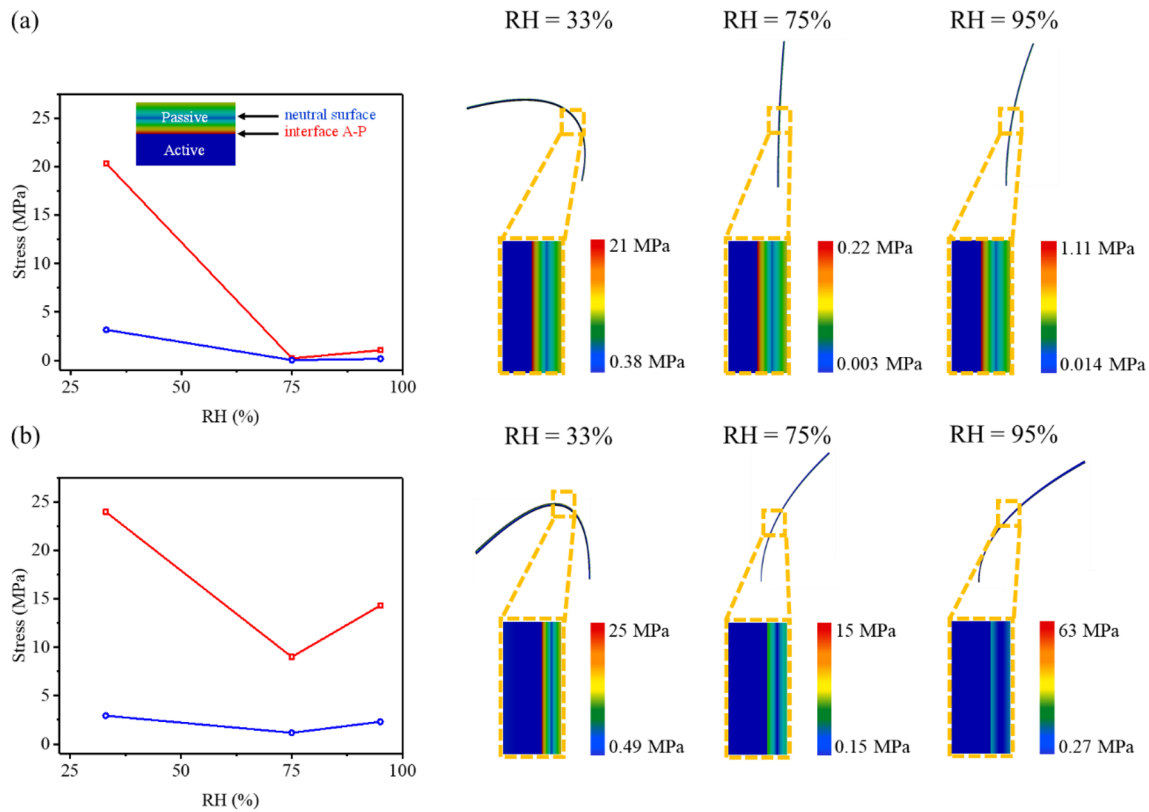


Fig. 11 The stress nephograms for bilayers model with passive to active layer thickness ratio ($m, T_p/T_a$) at 33%, 75% and 95% RH during adsorption. **a** $m = 1, T_p = 200 \mu\text{m}$ **b** $m = 0.5, T_p = 200 \mu\text{m}$

the production of hygrometer: convert bending curvature directly into an accurate humidity value, thereby eliminating the influence of the adsorption or desorption process. However, the limitations of the ability to withstand load and resistance to degradation limited the outdoor use. It is hoped that the follow-up study can be more in-depth in these aspects.

Abbreviations

RH	Relative humidity
RH_0	The critical relative humidity
iMC	Initial moisture content
FEA	Finite-element analysis
L	Longitudinal
R	Radial
T	Tangential
$m (T_p/T_a)$	Passive to active layer thickness ratio
T_p	Thickness of passive layer
T_a	Thickness of active layer
ΔK	Relative curvature

Acknowledgements

The authors are grateful for the financial support from the National Natural Science Foundation of China (No. 32171705, 32101454).

Author contributions

The authors confirm contribution to the paper as follows: data collection and investigation: HP, ZL; analysis and interpretation of results: JZ, JJ; draft

manuscript preparation: HP, JL, TZ. All the authors reviewed the results and approved the final version of the manuscript.

Funding

This research was sponsored by the National Natural Science Foundation of China (No. 32171705, 32101454).

Availability of data and materials

The raw/processed data required to reproduce these findings cannot be shared at this time as the data also form part of an ongoing study.

Declarations

Competing interests

The authors declare that they have no competing interests.

Received: 17 April 2023 Accepted: 25 August 2023

Published online: 07 September 2023

References

1. Skaar C (1988) Wood-water relations. Springer Verlag, Berlin
2. Eder M, Schäffner W, Burgert I, Fratzl P (2020) Wood and the Activity of Dead Tissue. Adv Mater 2001412
3. Grönquist P, Panchadcharam P, Wood D, Menges A, Rüggeberg M, Wittel FK (2020) Computational analysis of hygromorphic self-shaping wood gridshell structures. Roy Soc Open Sci 7:192210

4. Vailati C, Bachtiar E, Hass P, Burgert I, Rüggeberg M (2018) An autonomous shading system based on coupled wood bilayer elements. *Energy Buildings* 158:1013–1022
5. Durai Prabhakaran RT, Spear MJ, Curling S, Wootton-Beard P, Jones P, Donnison I, Ormondroyd GA (2019) Plants and architecture: the role of biology and biomimetics in materials development for buildings. *Intell Build Int* 11:178–211
6. Dawson C, Vincent JFV, Rocca A-M (1997) How pine cones open. *Nature* 390:668–668
7. Liu Z, Zhang Z, Ritchie RO (2020) Structural orientation and anisotropy in biological materials: functional designs and mechanics. *Adv Funct Mater* 30:1908121
8. Timoshenko S (1925) Analysis of bimetal thermostats. *J Opt Soc Am* 11:233–255
9. Reyssat E, Mahadevan L (2009) Hygromorphs: from pine cones to biomimetic bilayers. *J R Soc Interface* 6:951–957
10. Li SY, Wang KW (2017) Plant-inspired adaptive structures and materials for morphing and actuation: a review. *Bioinspir Biomim* 12:011001
11. Guiducci L, Razghandi K, Bertinetti L, Turcaud S, Rüggeberg M, Weaver JC, Fratzl P, Burgert I, Dunlop JWC (2016) Honeycomb actuators inspired by the unfolding of ice plant seed capsules. *PLoS ONE* 11:e0163506
12. Rüggeberg M, Burgert I (2015) Bio-inspired wooden actuators for large scale applications. *PLoS ONE* 10:e0120718
13. Péron M, Céline A, Jacquemin F, Le Duigou A (2020) Hygroscopic stresses in asymmetric biocomposite laminates submitted to various relative humidity conditions. *Compos Part A-Appl S* 134:105896
14. Bodig J, Jayne B (1982) *Mechanics of wood and wood composites*. Von Nostrand Reinhold Company, New York
15. Yang T, Mei C, Ma E, Cao J (2022) Effects of acetylation on moisture sorption of wood under cyclically changing conditions of relative humidity. *Eur J Wood Wood Prod* 81:723–731
16. Engelund ET, Thygesen LG, Svensson S, Hill CAS (2013) A critical discussion of the physics of wood–water interactions. *Wood Sci Technol* 47:141–161
17. Arévalo R, Hernández RE (2001) Influence of moisture sorption on swelling of mahogany (*Swietenia macrophylla* King) wood. *Holzforchung* 55:590–594
18. Yamamoto H, Sassus F, Ninomiya M, Gril J (2001) A model of anisotropic swelling and shrinking process of wood. *Wood Sci Technol* 35:167–181
19. Reichert S, Menges A, Correa D (2015) Meteorosensitive architecture: biomimetic building skins based on materially embedded and hygroscopically enabled responsiveness. *Comput Aided Design* 60:50–69
20. Grönquist P, Wittel F, Rüggeberg M (2018) Modeling and design of thin bending wooden bilayers. *PLoS ONE* 13:e0205607
21. Rindler A, Vay O, Hansmann C, Müller U (2017) Dimensional stability of multi-layered wood-based panels: a review. *Wood Sci Technol* 51:969–996
22. Grönquist P, Wood D, Hassani MM, Wittel FK, Menges A, Rüggeberg M (2019) Analysis of hygroscopic self-shaping wood at large scale for curved mass timber structures. *Sci Adv* 5:eaax1311
23. Wood D, Grönquist P, Bechert S, Aldinger L, Riggenbach D, Lehmann K, Rüggeberg M, Burgert I, Knippers JAN, Menges A (2020) From Machine Control to Material Programming: Self-Shaping Wood Manufacturing of a High Performance Curved CLT Structure—Urbach Tower. Paper presented at the FABRICATE 2020—Making Resilient Architecture, London, UK, April 2020
24. Holstov A, Bridgens B, Farmer G (2015) Hygromorphic materials for sustainable responsive architecture. *Constr Build Mater* 98:570–582
25. Menges A, Reichert S (2015) Performative wood: physically programming the responsive architecture of the hygroscope and hygroskin projects. *Archit Design* 85:66–73
26. Pelliccia G, Baldinelli G, Bianconi F, Filippucci M, Fioravanti M, Goli G, Rotili A, Togni M (2020) Characterisation of wood hygromorphic panels for relative humidity passive control. *J Build Eng* 32:101829
27. Kay R, Nitiema K, Correa Zuluaga D (2020) The Bio-inspired Design of a Self-propelling Robot Driven by Changes in Humidity. In: *Anthropologic: Architecture and Fabrication in the cognitive age—Proceedings of the 38th eCAADe Conference—Volume 2*, Berlin, Germany, pp 233–242
28. Tahouni Y, Kruger F, Poppinga S, Wood D, Pfaff M, Ruhe J, Speck T, Menges A (2021) Programming sequential motion steps in 4D-printed hygromorphs by architected mesostructure and differential hygro-responsiveness. *Bioinspir Biomim* 16:055002
29. Hill CAS, Keating BA, Jalaludin Z, Mahrdrdt E (2012) A rheological description of the water vapour sorption kinetics behaviour of wood invoking a model using a canonical assembly of Kelvin-Voigt elements and a possible link with sorption hysteresis. *Holzforchung* 66:35–47
30. Salmén L, Larsson PA (2018) On the origin of sorption hysteresis in cellulosic materials. *Carbohydr Polym* 182:15–20
31. Le Duigou A, Chabaud G, Scarpa F, Castro M. Bioinspired electro-thermo-hygro reversible shape-changing materials by 4D printing. *Adv Funct Mater* 0: 1903280
32. Le Duigou A, Castro M (2015) Moisture-induced self-shaping flax-reinforced polypropylene biocomposite actuator. *Ind Crop Prod* 71:1–6
33. Zhao C, Ren L, Song Z, Deng L, Liu Q (2019) Structure-driven biomimetic self-morphing composites fabricated by multi-process 3-D printing. *Compos Part A-Appl S* 123:1–9
34. Jauslin C, Pellicane PJ, Gutkowski RM (1995) Finite-element analysis of wood joints. *J Mater in Civil Eng* 7:50–58
35. Gui YQ, Jones EW, Taylor FW, Issa CA (1994) An application of finite element analysis to wood drying. *Wood Fiber Sci* 26:281–293
36. Le Duigou A, Keryvin V, Beaugrand J, Pernes M, Scarpa F, Castro M (2019) Humidity responsive actuation of bioinspired hygromorph biocomposites (HBC) for adaptive structures. *Compos Part A-Appl S* 116:36–45
37. Sar BE, Fréour S, Davies P, Jacquemin F (2012) Coupling moisture diffusion and internal mechanical states in polymers—a thermodynamical approach. *Eur J Mech A-Solid* 36:38–43
38. Le Duigou A, Castro M (2017) Hygromorph BioComposites: effect of fibre content and interfacial strength on the actuation performances. *Ind Crop Prod* 99:142–149
39. Biblis EJ (1970) Effect of thickness of microtome sections on their tensile properties. *Wood Fiber Sci* 2:19–30
40. Guo F, Altaner CM, Jarvis MC (2020) Thickness-dependent stiffness of wood: potential mechanisms and implications. *Holzforchung* 74:1079–1087
41. Hill CAS, Norton A, Newman G (2009) The water vapor sorption behavior of natural fibers. *J Appl Polym Sci* 112:1524–1537
42. Lu Y, Pignatello JJ (2004) History-dependent sorption in humic acids and a lignite in the context of a polymer model for natural organic matter. *Environ Sci Technol* 38:5853–5862
43. Salmén L (2004) Micromechanical understanding of the cell-wall structure. *C R Biol* 327:873–880

Publisher's Note

Springer Nature remains neutral with regard to jurisdictional claims in published maps and institutional affiliations.

Submit your manuscript to a SpringerOpen® journal and benefit from:

- Convenient online submission
- Rigorous peer review
- Open access: articles freely available online
- High visibility within the field
- Retaining the copyright to your article

Submit your next manuscript at ► [springeropen.com](https://www.springeropen.com)